Revisiting Theoretical Limits for One-Degree-of-Freedom Wave Energy Converters

Preprint

Nathan Tom

National Renewable Energy Laboratory

Presented at the 14th International Conference on Energy Sustainability
June 17–18, 2020

NREL is a national laboratory of the U.S. Department of Energy
Office of Energy Efficiency & Renewable Energy
Operated by the Alliance for Sustainable Energy, LLC

This report is available at no cost from the National Renewable Energy Laboratory (NREL) at www.nrel.gov/publications.

Contract No. DE-AC36-08GO28308

Conference Paper
NREL/CP-5000-75701
June 2020

Revisiting Theoretical Limits for One-Degree-of-Freedom Wave Energy Converters

Preprint

Nathan Tom

National Renewable Energy Laboratory

Suggested Citation
Tom, Nathan. 2020. *Revisiting Theoretical Limits for One-Degree-of-Freedom Wave Energy Converters: Preprint*. Golden, CO: National Renewable Energy Laboratory. NREL/CP-5000-75701. https://www.nrel.gov/docs/fy20osti/75701.pdf

Conference Paper
NREL/CP- 5000-75701
June 2020

National Renewable Energy Laboratory
15013 Denver West Parkway
Golden, CO 80401
303-275-3000 • www.nrel.gov

NOTICE

This work was authored in by the National Renewable Energy Laboratory, operated by Alliance for Sustainable Energy, LLC, for the U.S. Department of Energy (DOE) under Contract No. DE-AC36-08GO28308. Funding provided by the U.S. Department of Energy Office of Energy Efficiency and Renewable Energy Water Power Technologies Office. The views expressed herein do not necessarily represent the views of the DOE or the U.S. Government. The U.S. Government retains and the publisher, by accepting the article for publication, acknowledges that the U.S. Government retains a nonexclusive, paid-up, irrevocable, worldwide license to publish or reproduce the published form of this work, or allow others to do so, for U.S. Government purposes.

Cover Photos by Dennis Schroeder: (clockwise, left to right) NREL 51934, NREL 45897, NREL 42160, NREL 45891, NREL 48097, NREL 46526.

REVISITING THEORETICAL LIMITS FOR ONE-DEGREE-OF-FREEDOM WAVE ENERGY CONVERTERS

Nathan M. Tom *
National Wind Technology Center
National Renewable Energy Laboratory
Golden, Colorado, USA
E-mail: Nathan.Tom@nrel.gov

ABSTRACT

This work revisits the theoretical limits of one-degree-of-freedom wave energy converters. This paper considers the floating sphere used in the Ocean Energy Systems Task 10 Wave Energy Converter modeling and verification effort for analysis. Analytical equations are derived to determine bounds on the motion amplitude, time-averaged power, and power-take-off (PTO) force. A unique result was found that shows the time-averaged power absorbed by a wave energy converter can be defined solely by the inertial properties and radiation hydrodynamic coefficients. In addition, a unique expression for the PTO force amplitude was derived that has provided upper and lower bounds when resistive control is used to maximize power generation. For complex conjugate control, this same expression can only provide a lower bound, as there is theoretically no upper bound. These bounds are used to compare the performance of a floating sphere if it were to extract energy using surge or heave motion. The analysis shows that because of the differences in hydrodynamic coefficients of each oscillating mode, there will be different frequency ranges that provide better power capture efficiency. The influence of a motion constraint on power absorption while also utilizing a nonideal power take-off is examined and found to reduce the losses associated with bidirectional energy flow. The expression to calculate the time-averaged power with a nonideal PTO is modified by the mechanical-to-electrical efficiency and the ratio of the PTO spring and damping coefficients. The PTO spring and damping coefficients were separated in the expression, which allows for limits to be set on the possible values of PTO coefficients to ensure a net flow of power to the grid.

INTRODUCTION

Over the last 45 years since the publication of Salter's foundational paper on wave power [1], research and development in wave energy technologies has pushed forward in hopes of bringing the industry closer to commercialization. Over the past two decades, the worldwide marine and hydrokinetic energy sector has seen a resurgence in investment and research funding; however, it can be argued that the industry as a whole remains in the early stages of technology development. To date, there are still no commercially grid-connected wave energy converters (WECs) installed in the United States, with only a few megawatts installed worldwide [2]. A significant challenge with WEC technology is the conversion of slow, irregular, and high-force oscillatory motion to drive a generator with output quality that is acceptable for a utility grid network [3].

As a whole, the field of wave energy continues to host a wide diversity of technologies ranging in scale from paper concept to oceangoing prototype. Therefore, development funds can be spread thin across a diverse research portfolio that highlights the need for a structured innovation approach to facilitate an optimal convergence in WEC design and operation [4]. Although there are many different forms, WECs can generally be divided into three predominant classifications: 1) attenuator, 2) point absorber, and 3) terminator. Within these classifications,

*Address all correspondence to this author.

WEC devices can be further defined based on the mode of motion used to capture energy, such as point absorbers, oscillating wave surge converters, oscillating water columns, overtopping devices, and bulge wave devices [3]. Of all of the WEC concepts, the most common and well-studied design is the point absorber, which typically has a narrow-banded response; therefore, control is generally required to improve energy capture [5].

Often the point absorber is assumed to oscillate in heave with the wave elevation profile given the common buoy-like and bottom-referenced device concepts. However, as discussed in [6], the hydrodynamic radiation and diffraction forces between surging, similar for pitch, and heaving devices have different frequency responses that influence the effective energy capture bandwidth. For example, it is well known that the theoretical maximum power that can be captured by a surging or pitching device is twice that of a heaving device because of the asymmetric wave radiation pattern [7].

This paper builds off the work of [6] by extending the performance metric comparison to the required displacement amplitude and power-take-off (PTO) force, and considering nonideal conversion efficiency. After introducing the floating WEC used in this analysis, the author provides a discussion of the differences in the hydrodynamic and radiation coefficients. This is followed by deriving the upper bound on the amplitude of displacement for each mode of motion, highlighting how constraints such as the PTO stroke length can reduce the energy capture potential. Next, we discuss the influence of the hydrodynamic radiation coefficients on maximum power capture using complex conjugate [5] or resistive PTO control. This is followed by deriving the upper and lower bounds of the PTO force requirement, which depends on the control strategy implemented. Finally, we provide a discussion on how improvements in maximum power capture can be degraded by nonunity PTO efficiency, which can be aggravated based on the mode of oscillation.

FLOATING BODY DESCRIPTION

For this study, we selected the floating sphere used for the Ocean Energy Systems Task 10 Wave Energy Converter modeling and verification effort [8]. The floating sphere has a radius of 5.0 m, and its origin is located on the mean water surface at the center of the spherical body, with a summary of the model parameters provided in Table 1. The mass of a floating half-submerged sphere is given by:

$$m = \frac{2\rho\pi r^3}{3} \tag{1}$$

where ρ is the fluid density, and r is the sphere radius. The linearized heave hydrostatic restoring force coefficient is given by:

$$C_{33} = \rho g A_{wp} = \rho g \pi r^2 \tag{2}$$

Table 1. General Properties of the Floating Sphere [8]

Parameters	Variable	Assigned Values
Radius of Sphere	r	5 m
Center of Gravity	c_g	0.0, 0.0, -2.0 m
Center of Buoyancy	c_b	0.0, 0.0, -1.875 m
Mass of Sphere	m	$261.8\text{x}10^3$ kg
Water Depth	m	Infinite m
Water Density	ρ	1000 kg/m^3

where A_{wp} is the water plane area. A free floating body will not have a hydrostatic restoring coefficient in surge; however, for station keeping an external spring, such as mooring or PTO control strategies, it will need to be coupled to the surge degree of motion. For this analysis, we assumed that the floating sphere could be connected to a fixed reference frame by an external spring with a magnitude equal to the heave hydrostatic restoring coefficient (i.e., $C_{11} = C_{33}$).

The hydrodynamic coefficients used in the analysis to estimate the displacement and power absorption of the sphere were obtained from WAMIT [9] and are plotted in Fig. 1. As shown in Fig. 1(a), for heave oscillation the radiation wave damping peaks at a lower wave frequency than surge and the same for the added mass; however, for surge, the wave damping peak corresponds with a greater drop from the added mass peak than heave, which will be highlighted in a later section. For the wave-excitation force shown in Fig. 1(b), in heave the force is maximum at the lowest frequencies and continues to decrease as the wave frequency increases. While in surge, the wave-excitation force tends to zero at the upper and lower frequencies while peaking in the intermediate frequency regime. As will be discussed in a future section, as the WEC motion becomes more heavily constrained, the peak in power capture centers on the peak in the wave-excitation force rather than at the resonant frequency.

REGULAR WAVE ANALYSIS

In floating body dynamics, it is common practice to understand the frequency response of the device by analyzing the response under regular wave excitation, in which the incident wave elevation is described by:

$$\eta(x,t) = A\cos(\omega t - kx) = \Re\left\{Ae^{i\omega t}\right\} \tag{3}$$

where η is the wave elevation, A is the wave amplitude, ω is the wave angular frequency, and k is the wave number. For the time being, the mechanical force from the PTO system will be described by:

$$f_{PTOj} = -\Re\left\{(\lambda_g - iC_g/\omega)\, i\omega\xi_j e^{i\omega t}\right\} \tag{4}$$

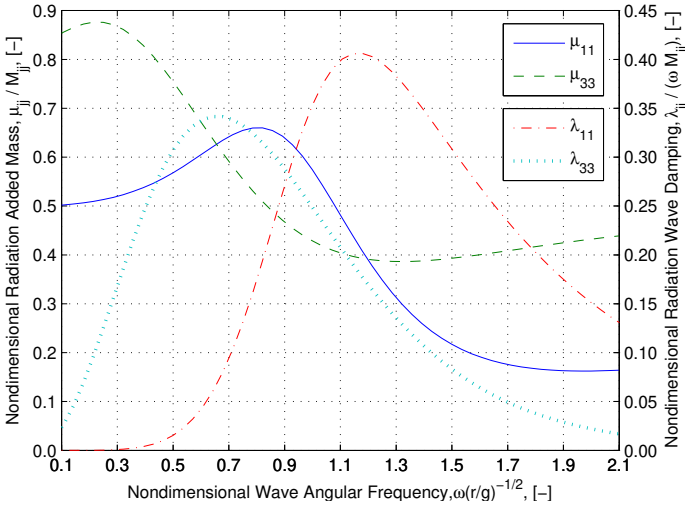

(a) Radiation Added Mass μ_{jj} and Wave Damping λ_{jj}

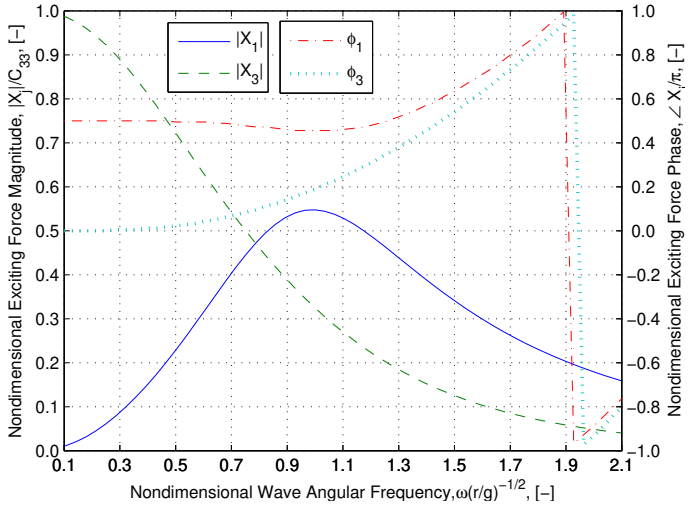

(b) Wave Exciting Force Magnitude $|X_j|$ and Phase ϕ_j

Figure 1. Nondimensional hydrodynamic surge and heave radiation and wave-excitation force coefficients for the floating sphere.

where C_g is the linear PTO-restoring coefficient, λ_g is the PTO linear-damping coefficient, and ξ_j is the complex amplitude of motion for the j^{th} degree of freedom.

The frequency-domain expressions for the hydrostatic, radiation, diffraction, and PTO forces can be inserted into the one-degree-of-freedom equation of motion to derive the displacement and velocity response amplitude operators of the floating sphere:

$$\frac{\xi_j}{A} = \frac{X_j}{[C_{jj}+C_g-\omega^2(M_{jj}+\mu_{jj})]+i\omega[\lambda_{jj}+\lambda_g]} \tag{5}$$

$$\frac{i\omega\xi_j}{A} = \frac{X_j}{[\lambda_{jj}+\lambda_g]+i[-(C_{jj}+C_g)/\omega+\omega(M_{jj}+\mu_{jj})]} \tag{6}$$

where X_j is the complex wave-exciting force per unit wave amplitude, C_{jj} is the restoring coefficient in the j^{th} degree of freedom, M_{jj} is the mass or moment of inertia in the j^{th} degree of freedom, μ_{jj} is the radiation added mass or added moment of inertia in the j^{th} degree of freedom, and λ_{jj} is the radiation wave damping in the j^{th} degree of freedom.

In order to obtain bounds on the motion amplitude for a given device, the magnitude of Eqn. (5) will be taken as follows:

$$\left|\frac{\xi_j}{A}\right| = \frac{|X_j|}{\sqrt{2}\omega\lambda_{jj}}\frac{1}{\Xi_j\sqrt{1+\frac{1}{\Xi_j}}} \tag{7}$$

$$= \frac{4\varepsilon\rho g V_g}{\sqrt{2}\omega k|X_j|}\frac{1}{\Xi_j\sqrt{1+\frac{1}{\Xi_j}}}\,,\ \varepsilon=\begin{cases}1 & \text{for } j=3\\ 2 & \text{for } j=1,\,5\end{cases}$$

where V_g is the wave group velocity, and the Haskind expression [10] has been substituted in the second line of Eqn. (7). Ξ is a measure of the ratio between the inertial and resistive forces that arise from WEC oscillation and is defined by:

$$\Xi_j = \sqrt{1+\left[\frac{C_{jj}+C_g-\omega^2(M_{jj}+\mu_{jj})}{\omega\lambda_{jj}}\right]^2} \tag{8}$$

Because the bracketed term in Eqn. (8) is squared, Ξ will be bounded between 1 and ∞; see Fig. 2. The lower bound will be obtained when the spring forces cancel the acceleration forces, and if no phase control is implemented, $C_g = 0$ will occur only at the natural frequency of the isolated floating body. Furthermore, it has also been assumed that the PTO linear damping coefficient has been selected, such that $\lambda_g = \lambda_{jj}\Xi$. The reason behind this selection will be described in the following section.

If deep water is assumed, $kh \geq \pi$, then Eqn. (7) can be simplified to the following form:

$$\left|\frac{\xi_j}{A}\right| = \frac{2\varepsilon\rho g}{\sqrt{2}k^2|X_j|}\underbrace{\frac{1}{\Xi_j\sqrt{1+\frac{1}{\Xi_j}}}}_{\Pi} = \frac{2\varepsilon\rho g^3}{\sqrt{2}\omega^4|X_j|}\Pi \tag{9}$$

$$= \frac{\varepsilon\rho g\lambda_w^2}{2\sqrt{2}\pi^2|X_j|}\Pi\,,\ \varepsilon=\begin{cases}1 & \text{for } j=3\\ 2 & \text{for } j=1,\,5\end{cases}$$

where λ_w is the wavelength, and h is the water depth. Because Eqn. (8) is bounded between $[1,\infty]$, the term, Π, in Eqn. (9) is bounded between $\left[0,1/\sqrt{2}\right]$; see Fig. 3. The upper bound on the motion response is set by the following expression:

$$\left|\frac{\xi_j}{A}\right|_{max} = \frac{\varepsilon\rho g\lambda_w^2}{4\pi^2|X_j|}\,,\ \varepsilon=\begin{cases}1 & \text{for } j=3\\ 2 & \text{for } j=1,\,5\end{cases} \tag{10}$$

Therefore, the maximum displacement amplitude, in deep water,

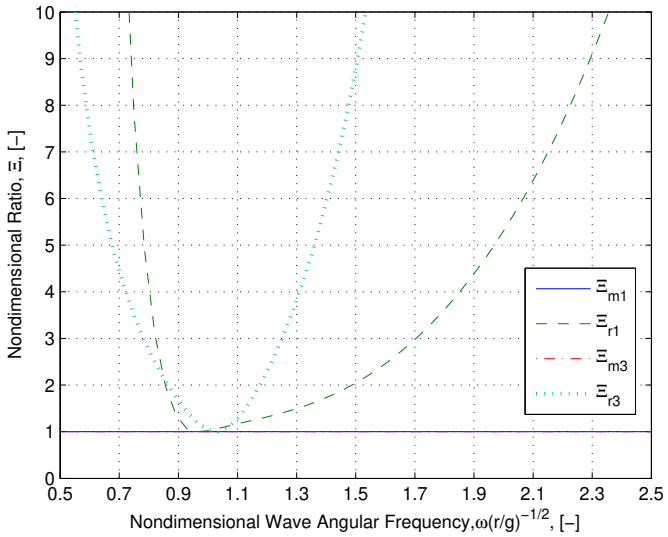

Figure 2. The values of Ξ, given by Eqn. (8), which is a measure of the ratio between inertial/spring and resistive forces that are generated because of WEC oscillations. The subscript m refers to maximum power absorption, and the subscript r refers to the maximum power absorption under resistive control when setting $C_g = 0$.

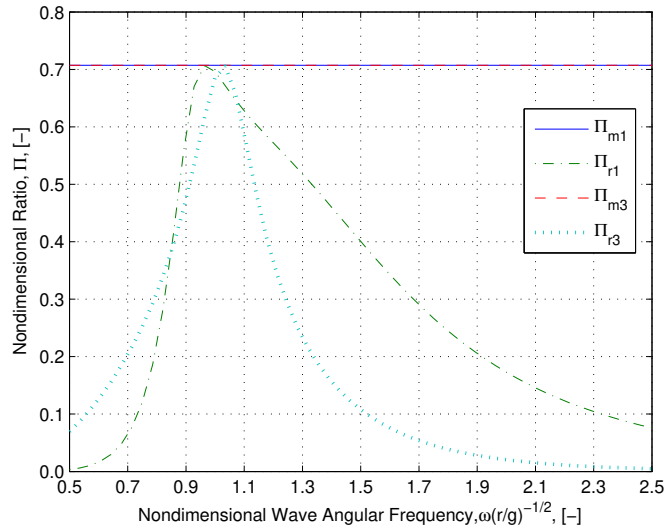

Figure 3. The values of Π, defined in Eqn. (9). The subscript m refers to maximum power absorption, and the subscript r refers to the maximum power absorption under resistive control when setting $C_g = 0$.

is proportional to the wavelength squared and inversely proportional to the wave-exciting force/torque.

If shallow water is assumed, $kh \to 0$, then Eqn. (7) can be simplified to the following form:

$$\left|\frac{\xi_j}{A}\right|_{max} = \frac{2\varepsilon\rho g^2 h}{\omega^2 |X_j|}\,,\ \varepsilon = \begin{cases} 1 & \text{for } j = 3 \\ 2 & \text{for } j = 1,\ 5 \end{cases} \tag{11}$$

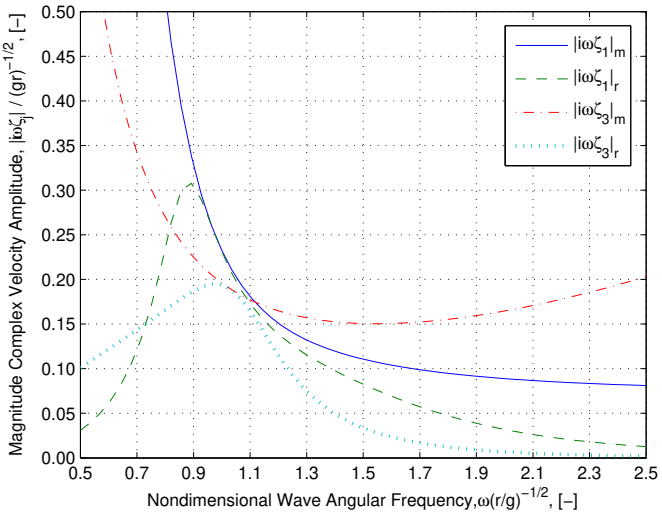

Figure 4. Nondimensional surge and heave velocity response amplitude operators for the floating sphere. The subscript m refers to maximum power absorption, and the subscript r refers to the maximum power absorption under resistive control when setting $C_g = 0$.

The maximum motion displacement amplitude in shallow water is proportional to the water depth, and inversely proportional to the wave-exciting force and to the wave angular frequency squared.

When comparing the velocity amplitudes between surge and heave in deep water for maximum power capture, see Fig. 4; for wave frequencies below the resonance frequency, surge outpaces heave. Above the resonance frequency, the surge oscillation requires a smaller amplitude compared to heave that is consistent with Eqn. (10), as the wave-excitation force is one variable that differs between the two oscillation modes. Referring back to Fig. 1(b), one can see that the surge wave-excitation force is larger than heave for higher frequencies and will reduce the required displacement amplitude.

Time-Averaged Power Absorption

The maximum time-averaged power absorbed by a WEC oscillating in a single degree of freedom [7] can be modeled by the following:

$$\frac{P_{Tj}}{A^2} = \frac{\lambda_g \left|i\omega\xi_j\right|^2}{2} = \frac{1}{4}\frac{|X_j|^2}{\lambda_{jj}} \frac{1}{1+\sqrt{1+\left(\frac{C_{jj}+C_g-\omega^2\left(M_{jj}+\mu_{jj}\right)}{\omega\lambda_{jj}}\right)^2}}$$

$$= \frac{1}{4}\frac{|X_j|^2}{\lambda_{jj}} \frac{1}{1+\Xi_j} \tag{12}$$

Therefore, it is beneficial to minimize the variable Ξ ratio, which can be described by the following inequality:

$$\left(C_{jj}+C_g\right)/\omega - \omega\left(M_{jj}+\mu_{jj}\right) << \lambda_{jj} \tag{13}$$

As described earlier in the floating body description section, given that the hydrostatic restoring coefficient is static, then the power capture potential of the WEC will be greater when the radiation added mass is minimized and the wave damping is maximized. Thus, it may be possible to adjust the shape of a WEC at each wave frequency to meet the inequality by controlling the radiation added mass and wave damping coefficients.

The previously mentioned expressions require unconstrained motion, and the PTO linear damping coefficient takes the following value:

$$\lambda_g = \lambda_{jj}\sqrt{1+\left[\frac{C_{jj}+C_g-\omega^2\left(M_{jj}+\mu_{jj}\right)}{\omega\lambda_{jj}}\right]^2} = \lambda_{jj}\Xi \quad (14)$$

Eqn. (12) can be simplified further by substituting the Haskind expression, as follows:

$$\frac{P_{Tj}}{A^2} = \frac{\varepsilon\rho g V_g}{k}\underbrace{\frac{1}{1+\Xi_j}}_{\chi} \quad , \quad \varepsilon = \begin{cases} 1 & \text{for } j=3 \\ 2 & \text{for } j=1,\ 5 \end{cases} \quad (15)$$

As shown by Eqn. (15), the WEC time-averaged power can be defined solely by the inertial properties and the radiation hydrodynamic coefficients. The expression for the time-averaged power now requires fewer hydrodynamic coefficients to evaluate the maximum power potential of a given WEC. The power absorption of a floating body can be estimated from the value of χ, which is plotted in Fig. 5. In addition, the theoretical maximum power absorption limit for an axisymmetric device, which is oscillating in pitch or surge, is twice that of the heaving case [7,11].

The maximum power absorption from Eqn. (15) is obtained when $\Xi_j = 1$, which occurs when the inertial and spring forces cancel. This condition is naturally met when the wave frequency matches the resonance frequency of the floating body [7]. As the wave frequency moves either above or below the resonance frequency, an external positive or negative PTO spring, equal to $C_g = -\left[C_{jj}-\omega^2\left(M_{jj}+\mu_{jj}\right)\right]$, must be added to the WEC system to obtain maximum power absorption and is often referred to as complex conjugate control [11]. Incorporating this controllable spring remains a current research interest in the wave energy field, with several efforts implementing the spring either mechanically or through control strategies. Because of the increased complexity related to incorporating a controllable spring, many developers have relied on resistive control by adjusting the PTO damping coefficient, λ_g, which is equal to Eqn. (14), when setting $C_g = 0$.

The power absorption obtained from complex conjugate and resistive control is equal at the resonance frequency of the floating body; however, it is of interest to develop a ratio between these two control strategies at other wave frequencies. The ratio can be calculated by taking the ratio of Eqn. (15) when setting

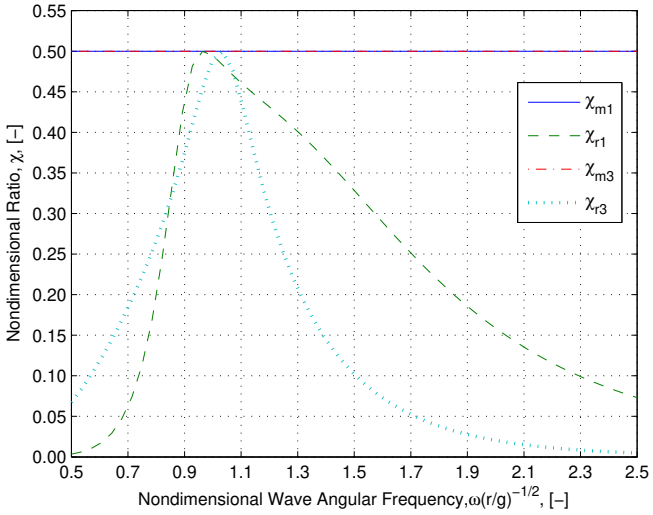

Figure 5. The values of χ, defined in Eqn. (15). The subscript m refers to maximum power absorption, the subscript r refers to the maximum power absorption under resistive control when setting $C_g = 0$.

$\Xi_j = 1$ and with Ξ_j when $C_g = 0$, which provides the following expression:

$$\frac{P_{Tmj}}{P_{Trj}} = \frac{1+\Xi_{rj}}{2} = \frac{1+\sqrt{1+\left[\frac{C_{jj}-\omega^2\left(M_{jj}+\mu_{jj}\right)}{\omega\lambda_{jj}}\right]^2}}{2} \quad (16)$$

where the subscript m refers to maximum power absorption, whereas the subscript r refers to the maximum power absorption under resistive control, and Ξ_{rj} refers to setting $C_g = 0$ in Eqn. (8). Equation (16) has been plotted in Fig. 6 and is unique in that it remains dependent only on the spring, inertial, and radiation coefficients. Furthermore, as shown in Fig. 6, when above the resonance frequencies, the ratio between complex conjugate and resistive control strategies is much lower for surge than in heave, whereas below resonance surge will quickly outpace heave. This performance can be attributed to the natural hydrodynamic bandwidth, which helps tune the power capture, as discussed in [6].

Incident Wave Power and Capture Width

To provide a measure of the capture efficiency for a given WEC, the time-averaged power contained within a propagating wave must be calculated. The time-averaged wave-power-per-unit width, P_w, can be calculated from the following equation:

$$\begin{aligned} \frac{P_w}{A^2} &= \frac{1}{2}\rho g V_g = \frac{1}{4}\rho g\sqrt{\frac{g}{h}\tanh kh}\left[1+\frac{2kh}{\sinh 2kh}\right] \\ &\overbrace{=}^{kh\to\infty} \frac{1}{4}\frac{\rho g^2}{\omega} = \frac{\rho g^2 T}{8\pi} \end{aligned} \quad (17)$$

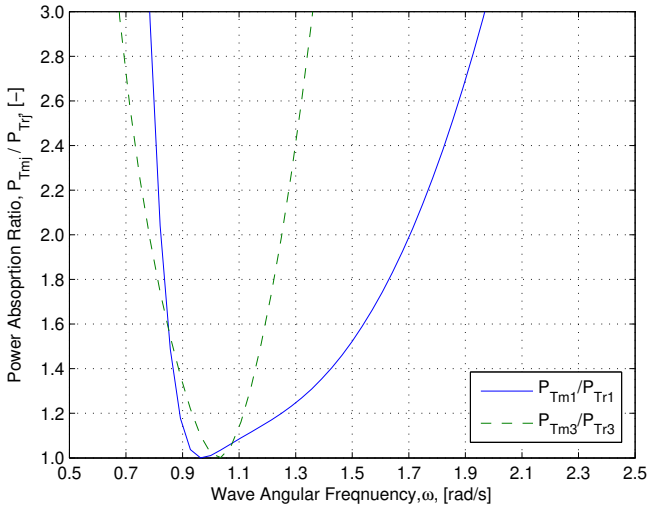

Figure 6. Ratio of power absorption between complex conjugate and resistive control for the floating sphere.

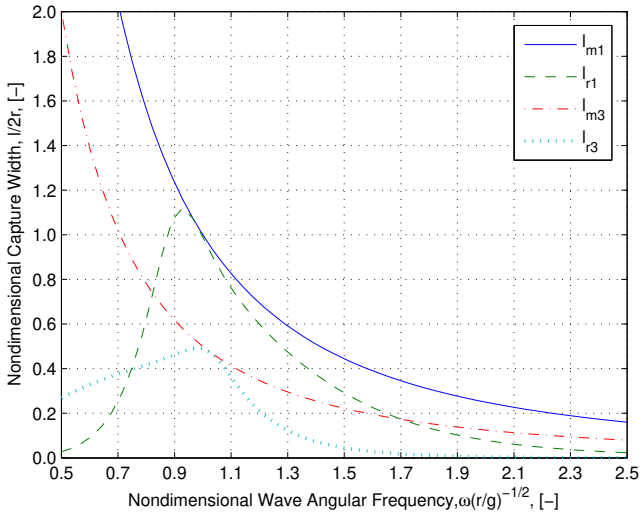

Figure 7. The capture width of complex conjugate and resistive control nondimensionalized by the diameter of the floating sphere.

where T is the wave period. The capture width is normally defined as the ratio of the time-averaged WEC absorbed to the wave power and given as:

$$l_j = \frac{P_{Tj}}{P_w} \tag{18}$$

Equations (15) and (17) can be substituted into Eqn. (18) to calculate the capture width of a given WEC:

$$l_j = \frac{\frac{\varepsilon \rho g V_g}{k}\frac{1}{1+\Xi_j}}{\frac{1}{2}\rho g V_g} = \frac{2\varepsilon}{k}\frac{1}{1+\Xi_j} \tag{19}$$

$$\max l_j = \frac{\varepsilon}{k} = \frac{\varepsilon \lambda_w}{2\pi} \quad , \quad \varepsilon = \begin{cases} 1 & \text{for } j = 3 \\ 2 & \text{for } j = 1,\ 5 \end{cases} \tag{20}$$

The maximum capture width is related to the wavelength, which theoretically implies that a WEC can absorb more incident wave power than contained within the WEC length that is perpendicular to the wave crest (see Fig. 7); however, it is well known that the required amplitudes of motion may not be physically achieved [7]. The results from Eqn. (19) are limited to axisymmetric devices, but if the device characteristic length is small compared to the wavelength, the device could be treated as a point absorber with antisymmetrical wave radiation patterns [14].

Maximum Absorbed Power Under Motion Constraints

The theoretical maximum WEC power absorption, given by Eqn. (12), requires unconstrained motion and is known to require unrealistic amplitudes of motion. As observed from Eqn. (10), the required displacement amplitude will quickly increase in longer wave periods [7], where the wavelength can be several hundred meters. Therefore, the maximum power absorption under motion amplitude constraints, while assuming sinusoidal motion, was explored in [12], which provides the following expression:

$$P_{Tj} = \begin{cases} \frac{1}{8}A^2 \left|X_j\right|^2 / \lambda_{jj} & \delta_j \geq 1 \\ \frac{1}{2}A \left|X_j\right| \omega \left|\xi_j\right|_{max} - \lambda_{jj}\omega^2 \left|\xi_j\right|^2_{max} & \delta_j < 1 \end{cases} \tag{21}$$

where $\left|\xi_j\right|_{max}$ is the maximum motion displacement amplitude, and δ is the ratio between the constrained-to-optimal velocity given by:

$$\delta_j = \frac{\omega \left|\xi_j\right|_{max}}{A}\frac{2\lambda_{jj}}{\left|X_j\right|} = \frac{\omega \left|\xi_j\right|_{max}}{A}\frac{k\left|X_j\right|}{2\varepsilon\rho g V_g} \tag{22}$$

To match the power output described earlier, for $\delta_j < 1$, the required linear PTO coefficients are given by:

$$\frac{\lambda_g}{\lambda_{jj}} = \begin{cases} 1 \ , & \delta_j \geq 1 \\ \frac{A\left|X_j\right|}{\omega\left|\xi_j\right|_{max}\lambda_{jj}} - 1 \ , & \delta < 1 \end{cases} \tag{23}$$

$$C_g = -\left[C_{jj} - \omega^2\left(M_{jj} + \mu_{jj}\right)\right] \tag{24}$$

If Eqn. (21), with $\delta_j < 1$, was substituted into the numerator of Eqn. (18), the capture width would be inversely proportional to the wave amplitude. For unconstrained motion, which may correspond to a very small incident wave amplitude, the capture width will be invariant to the incident wave height; whereas for strongly constrained motion, which may also correspond to a very large incident wave amplitude, the capture width will be inversely proportional to the incident wave height and become less efficient from the hydrodynamic perspective. In taking the

limit, $\delta \to 0$, the absorbed power is maximized at the frequency with the greatest wave-exciting force/torque rather than at the resonance frequency [13].

Peak-to-Average Power Ratio

The instantaneous power absorbed by an ideal power-take-off unit [15] can be modeled as follows:

$$P_j(t) = \frac{\lambda_g \left|i\omega\xi_j\right|^2}{2} + \frac{\left|i\omega\xi_j\right|^2}{2}|Z|\cos\left(2\left(\omega t + \phi\right) + \nu\right) \quad (25)$$

where $Z = \lambda_g - iC_g/\omega$, ν is the phase angle of Z, and ϕ is the phase angle of $i\omega\xi_j$. As observed in the second term in Eqn. (25), if $C_g \neq 0$, the instantaneous power will fluctuate between negative and positive values, indicating a reversal of the energy flow. The peaks in the PTO instantaneous absorbed power (P_{+j}) and the reactive input power (P_{-j}) are given by:

$$P_{\pm j} = \frac{\lambda_g |i\omega\xi_j|^2}{2}\left[1 \pm \sqrt{1 + \left(\frac{C_g}{\omega\lambda_g}\right)^2}\right] \quad (26)$$

The peak-to-average power ratio for the WEC can be obtained by dividing Eqn. (26) by the time-averaged power, as shown in Eqn. (12), leading to the following expression:

$$PA_{\pm j} = 1 \pm \sqrt{1 + \left(\frac{C_g}{\omega\lambda_g}\right)^2} \quad (27)$$

Therefore, the PTO peak-to-average power ratio is defined only by the PTO force coefficients and can be tuned to stay within the power capacity of the PTO. As observed from Eqn. (27), there will be no bidirectional energy flow when $C_g = 0$, preventing any negative instantaneous power. This condition is often referred to as resistive control, and the peak-to-average power ratio will be 2. The input power requirement, $C_g \neq 0$, is also naturally eliminated at the resonance frequency of the isolated floating body; however, as the wave frequency moves away from resonance, the peak-to-average power ratio quickly increases, resulting in large swings in bidirectional energy flow.

If bidirectional energy flow is allowed and the PTO force coefficients, C_g and λ_g, are selected such that the phase and amplitude conditions required for optimum power extraction are achieved [11]—refer to Eqn. (23) and Eqn. (24)—then the peak-to-average power ratio can be calculated from the following expression:

$$\begin{aligned} PA_{\pm j} &= 1 \pm \sqrt{1 + \left[\frac{C_{jj} - \omega^2\left(M_{jj} + \mu_{jj}\right)}{\omega\lambda_{jj}}\right]^2} \\ &= 1 \pm \Xi_{rj} \end{aligned} \quad (28)$$

Equation (28) requires unconstrained motion and has been plotted in Fig. 8, but can be adapted to account for motion constraints, similar to Eqn. (21). If the expression for the linear PTO damping coefficient, when $\delta_j < 1$, is inserted into Eqn. (27), the following expression is obtained:

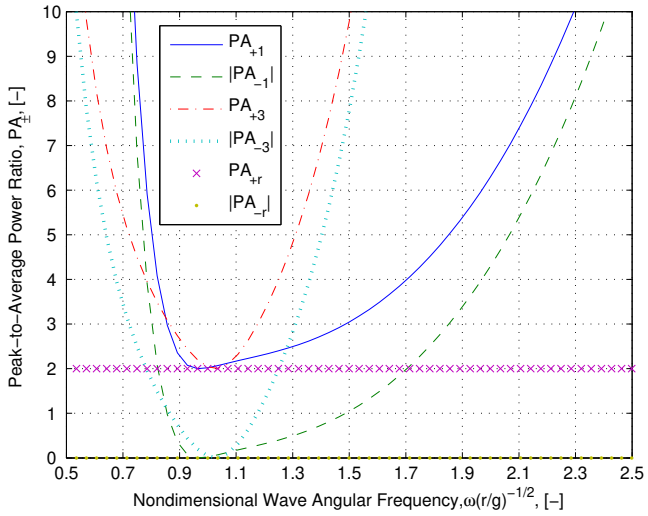

Figure 8. The peak-to-average power ratio for complex conjugate and resistive control of the floating sphere.

$$\begin{aligned} PA_{\pm j} &= 1 \pm \sqrt{1 + \left[\frac{C_{jj} - \omega^2\left(M_{jj} + \mu_{jj}\right)}{\omega\left(\frac{A|X_j|}{\omega|\xi_j|_{max}} - \lambda_{jj}\right)}\right]^2} \\ &= 1 \pm \sqrt{1 + \left[\frac{C_{jj} - \omega^2\left(M_{jj} + \mu_{jj}\right)}{A\left(1 - \frac{\delta_j}{2}\right)\frac{|X_j|}{|\xi_j|_{max}}}\right]^2} \end{aligned} \quad (29)$$

where, as the wave amplitude increases, all terms are constant except for A and δ_j. However, as A increases, δ_j decreases, which provides a nonlinear increase in the denominator under the square root. As the linear PTO damping coefficient is increased to meet a given displacement constraint, the peak-to-average power ratio will be reduced, and the reduction is nonlinearly proportional to the increase in wave amplitude.

Power-Take-Off Force

For the WEC system to capture energy, a PTO unit must be included to provide a resistive force that acts against WEC motion. The complex PTO force amplitude, α_j, in the frequency domain can be expressed as:

$$\begin{aligned} \frac{\alpha_j}{A} &= \frac{\left[C_g + i\omega\lambda_g\right]X_j}{\left[C_{jj} + C_g - \omega^2\left(M_{jj} + \mu_{jj}\right)\right] + i\omega\left[\lambda_g + \lambda_{jj}\right]} \\ &= -\left[\lambda_g - iC_g/\omega\right]i\omega\xi_j = Z_{uj}i\omega\xi_j \end{aligned} \quad (30)$$

where α_j is the complex PTO force/torque amplitude depending on the degree of freedom used to extract the incident wave power, and Z_{uj} is the PTO force-to-velocity transfer function. In order to estimate the magnitude of the force amplitude required by the PTO, we take the absolute value of Eqn. (30) and divide it by $\omega\lambda_{jj}$:

$$\left|\frac{\alpha_j}{A}\right| = \frac{\sqrt{\left[\frac{C_g}{\omega\lambda_{jj}}\right]^2 + \left[\frac{\lambda_g}{\lambda_{jj}}\right]^2}}{\sqrt{\left[\frac{C_{jj}+C_g-\omega^2\left(M_{jj}+\mu_{jj}\right)}{\omega\lambda_{jj}}\right]^2 + \left[\frac{\lambda_g}{\lambda_{jj}}+1\right]^2}}\left|X_j\right| \quad (31)$$

$$= \frac{\sqrt{1+\left[\frac{C_g}{\omega\lambda_g}\right]^2}}{\sqrt{1+2\left[\frac{\lambda_{jj}}{\lambda_g}\right]+\Xi^2\left[\frac{\lambda_{jj}}{\lambda_g}\right]^2}}\left|X_j\right| \quad (32)$$

If bidirectional energy flow is allowed, then the optimum phase and amplitude conditions required for maximum power extraction can be met [11], and the complex PTO force/torque amplitude can be simplified as the following expression:

$$\left|\frac{\alpha_j}{A}\right| = \frac{\left|X_j\right|}{2}\sqrt{1+\left[\frac{C_{jj}-\omega^2\left(M_{jj}+\mu_{jj}\right)}{\omega\lambda_{jj}}\right]^2} = \frac{\left|X_j\right|\Xi_{rj}}{2} \quad (33)$$

The second term under the square root in Eqn. (33) will always be greater than or equal to 0, resulting in the square root having a lower bound of 1 and an unconstrained upper bound. The lower bound will only be met when the wave frequency is equal to the resonance frequency of the isolated floating body. Therefore, the expected PTO force under the optimum conditions for power extraction will always be greater than half of the wave-exciting force.

If bidirectional energy flow is prohibited, $C_g = 0$, and the PTO damping coefficient is selected to optimize power absorption (refer to Eqn. (8), the required PTO force will be expressed as follows:

$$\left|\frac{\alpha_j}{A}\right| = \frac{\sqrt{2}}{2}\left|X_j\right|\sqrt{\frac{\Xi_j}{1+\Xi_j}} = \begin{cases} \frac{\left|X_j\right|}{2} & \text{as } \Xi_j \to 0 \\ \frac{\sqrt{2}}{2}\left|X_j\right| & \text{as } \Xi_j \to \infty \end{cases} \quad (34)$$

For resistive control, the PTO force amplitude will vary between $1/2$ and $\sqrt{2}/2$ of the wave-exciting force; see Fig. 9. Equations (33) and (34) converge to the same value when the wave frequency matches the resonant frequency of the isolated floating body, as the conditions for optimum power extraction are met by both control schemes.

The magnitude and phase relationship of the PTO force-to-velocity transfer function can be expressed as follows:

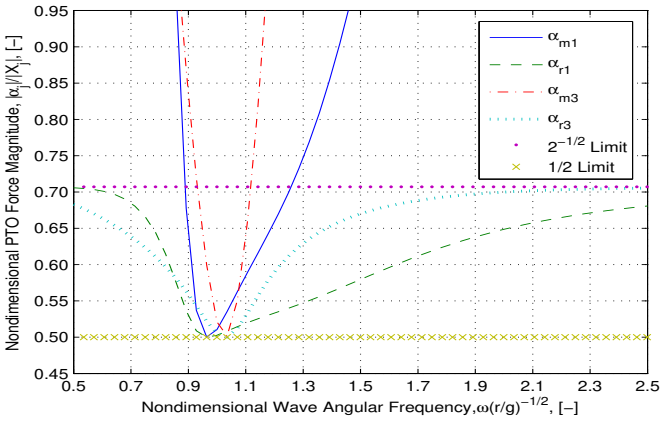

Figure 9. The nondimensional power take-off force amplitude for complex conjugate and resistive control of the floating sphere.

$$\angle Z_{uj} = \arctan\left(\frac{\Im\left\{Z_{uj}\right\}}{\Re\left\{Z_{uj}\right\}}\right) = \arctan\left(-\frac{C_g}{\omega\lambda_g}\right) \quad (35)$$

whereas under complex conjugate control, the phase angle will take the following form:

$$\angle Z_{uj} = \arctan\left(-\frac{\omega\left[M_{jj}+\mu_{jj}\right]-C_{jj}/\omega}{\lambda_{jj}}\right) \quad (36)$$

The phase angle between the PTO force and WEC velocity is bounded between $\pi/2$ ($\omega \to 0$) and $3\pi/2$ ($\omega \to \infty$) and crosses π at the resonance frequency of the WEC, as shown in Fig. 10. As shown in Fig. 11, the phase angle of the optimal PTO force-to-velocity transfer function deviates from π, which corresponds to resistive control. The linear trace between the WEC velocity-to-PTO force for resistive control is no longer optimum and becomes more oblong as the ratio of the imaginary-to-real component of Z_{uj}. At the limits of $\angle Z_{uj} = \pm\pi/2$, the control command has the largest force demand when the WEC is moving at the lowest speed. Requiring high forces at low speeds can lead to issues with conversion efficiency, as the PTO systems are not designed for optimum performance in this operating regime. Therefore, the gains over resistive control when applying complex conjugate control can be degraded with potential negative energy capture [16]. As observed in Fig. 10, at frequencies above resonance the phase angle for the heave oscillation mode decays more quickly to $3\pi/2$ than surge. Therefore, even when off resonance the surge oscillation mode requires less of a control action to tune the response of the WEC for optimum power capture, as long as the PTO is able to generate the required force.

Nonideal Power-Take-Off Efficiency

Complex conjugate control requires a two-way energy flow between the oscillating body and an energy storage system,

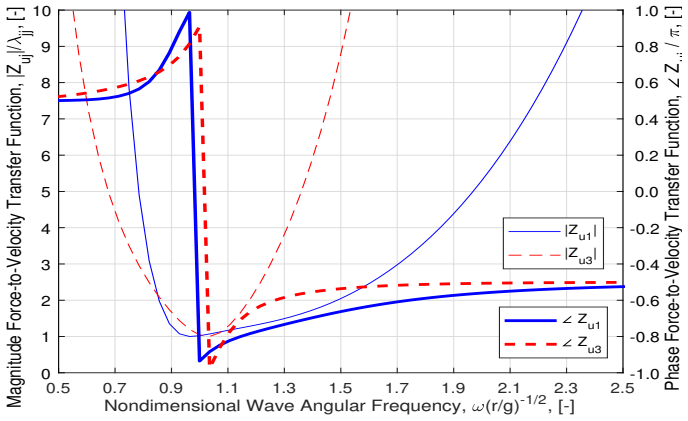

Figure 10. The magnitude and phase of the PTO force-to-velocity transfer function for complex conjugate control.

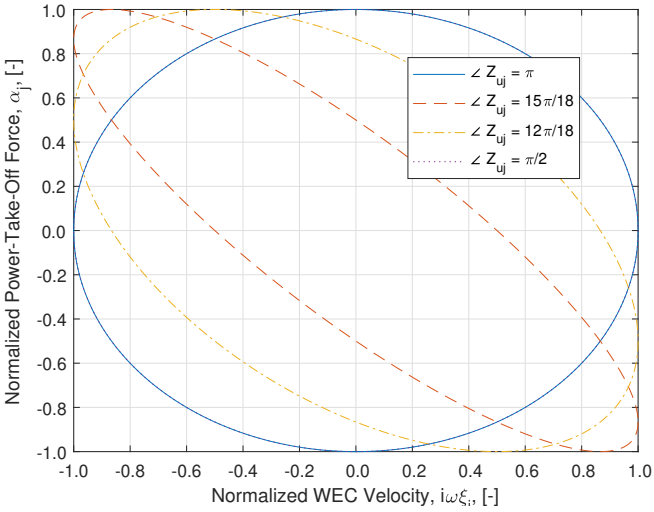

Figure 11. Plot of the changing relationship between velocity and force with changing phase angle.

which will have losses associated with the energy flux-reversal process if the PTO has a mechanical-to-electrical efficiency less than unity. If a PTO unit is selected, with a time-invariant mechanical-to-electrical efficiency defined by η_e, the resulting PTO output time-averaged power [16, 17] is given by:

$$P_O = \eta_e \frac{\lambda_g |i\omega\xi_j|^2}{2}\left[1 + e^* g^*\right], \quad e^* = \frac{1-\eta_e^2}{\eta_e^2} \quad , \tag{37}$$

$$g^* = \frac{2G^* - \sin 2G^* - 2G\left(1-\cos^2 G^*\right)}{2\pi} \quad , \tag{38}$$

$$G = \left|\frac{C_g}{\omega\lambda_g}\right|, \quad G^* = \arctan G \tag{39}$$

where P_O is the time-averaged power, after accounting for the efficiency steps in the power conversion chain, which can be sent to the grid. The nonideal PTO peak-to-average power ratios, $PA_{\eta_e\pm}$,

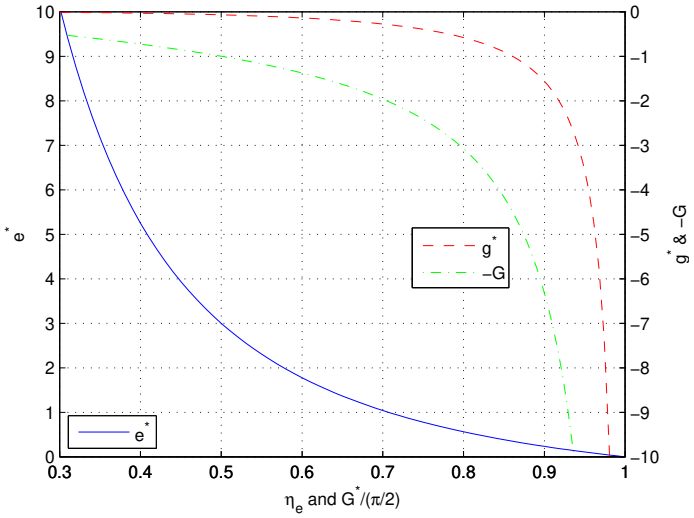

Figure 12. The effect on e^* and g^* for a range of η_e and G values.

can now be calculated from:

$$PA_{\eta_e+} = \frac{1+\sqrt{1+G^2}}{\left[1+e^* g^*\right]} \quad , \quad PA_{\eta_e-} = \frac{1-\sqrt{1+G^2}}{\eta_e^2\left[1+e^* g^*\right]} \tag{40}$$

The variation of the terms e^* and g^* in Eqn. (37), with respect to the PTO coefficient ratio, are plotted in Fig. 12. It can be observed from Eqn. (39) that the variable, G, is bounded between $[0, \infty]$ and that G^* is bounded between $[0, \pi/2]$. As observed in Fig. 12, the variable, $e^* \geq 0$, while $g^* \leq 0$, resulting in the bracketed term in Eqn. (37) being bounded by $[1, -\infty]$. When the value in brackets falls below 0, there is a net flow of energy to the device rather than the grid. Inclusion of the mechanical-to-electrical efficiency can greatly reduce the time-averaged output power if care is not taken in limiting G. A new ratio of the time-averaged output power, when considering nonideal PTO efficiency between the two control strategies, can be calculated by taking the ratio of Eqn. (37) when setting $\Xi_j = 1$ and with Ξ_j when $C_g = 0$, leading to the following expression:

$$\frac{P_{Omj}}{P_{Orj}} = \frac{1+\Xi_{rj}}{2}\left[1+e^* g^*\right] \tag{41}$$

As e^* and g^* are independent and can be separated in Eqn. (37), it is possible to set maximum limits on G to ensure net flow of power to the grid (tabulated in Table 2). Table 2 shows that, as the PTO mechanical-to-electrical efficiency is reduced, the maximum G value for a net power output is reduced at a much greater rate. Equation (41) only requires the radiation coefficients, and the natural hydrodynamic bandwidth of the device will play a role in tempering the negative effects of PTO efficiency. Therefore, we can expect the surge oscillation mode to be less sensitive than heave when considering PTO efficiency.

Table 2. Limits on G as a function of η_e

η_e	e^*	$G_{e^*g^*=-1/4}$	$G_{e^*g^*=-1/2}$	$G_{e^*g^*=-1}$
0.70	1.04	1.82	2.73	4.36
0.80	0.56	2.60	4.12	7.01
0.90	0.23	4.71	8.14	14.89
0.95	0.11	8.73	16.04	30.60

Conclusion

This paper explores the theoretical one-degree-of-freedom limits for a demonstrative floating spherical WEC. The dynamic response of the WEC considered both surge and heave modes of oscillation, as the differences in the hydrodynamic coefficients for different frequency ranges may lead to improved power capture efficiency. This follows the concept of a natural hydrodynamic bandwidth that has been shown to improve tuning of the WEC system for maximum power capture for the surge mode of motion compared to heave; however, this work does not suggest that heaving WECs are poorly designed, only that additional consideration should be taken when designing the floating body. As the work in this paper shows, the benefits of proper hydrodynamic tuning can significantly reduce the control strategy burden to maximize power capture, which can be degraded further when considering the PTO efficiency. Furthermore, to the best of our knowledge, a unique analytical expression for the PTO force amplitude was derived that provides upper and lower bounds that depend only on the wave-exciting force. Such bounds allow for rapid design iteration, as they eliminate the need to complete higher-fidelity simulations and can be calculated using frequency domain techniques. Furthermore, analytical bounds have been placed on the ratio of the PTO spring and damping coefficients, when considering PTO efficiency, to ensure a net power output that is also strongly influenced by the natural hydrodynamic bandwidth. The final decision in selecting the WEC mode of oscillation will be completed based on the designer vision and must also consider other external factors, such as station keeping, extreme loading, power-take-off selection, and maintenance windows.

ACKNOWLEDGMENT

This work was authored by the National Renewable Energy Laboratory, operated by Alliance for Sustainable Energy, LLC, for the U.S. Department of Energy (DOE) under Contract No. DE-AC36-08GO28308. Funding provided by the U.S. Department of Energy Office of Energy Efficiency and Renewable Energy Water Power Technologies Office. The views expressed in the article do not necessarily represent the views of the DOE or the U.S. Government. The U.S. Government retains and the publisher, by accepting the article for publication, acknowledges that the U.S. Government retains a nonexclusive, paid-up, irrevocable, worldwide license to publish or reproduce the published form of this work, or allow others to do so, for U.S. Government purposes.

REFERENCES

[1] Salter, S. H., 1974, "Wave power," *Nature*, 249, 720–724.

[2] Lehmann, M., Karimpour, F., Goudey, C. A., Jacobson, P. T., and Alam, M.-R., 2017, "Ocean wave energy in the United States: Current status and future perspectives," *Renewable and Sustainable Energy Reviews*, 74, 1300–1313.

[3] Drew, B., Plummer, A. R., and Sahinkaya, M. N., 2016, "A review of wave energy converter technology," *Proceedings of the Institution of Mechanical Engineers, Part A: Journal of Power and Energy*, 223 (8), 887–902.

[4] Weber, J., Costello, R., and Ringwood, J., 2013, "WEC technology performance levels (TPLs) - Metric for successful development of economic WEC technology," Proceedings of the 10th European Wave and Tidal Energy Conference, Aalborg, Denmark, Sept. 2–5.

[5] Ringwood, J., Bacelli, G., and Fusco, F., 2014, "Energy-maximizing control of wave-energy converters: The development of control system technology to optimize their operation," *IEEE Control Systems Magazine*, 34 (5), 30–55.

[6] Folley, M., Henry, A., and Whittaker, T., 2015, "Contrasting the hydrodynamics of heaving and surging wave energy converters," Proceedings of the 11th European Wave and Tidal Energy Conference, Nantes, France, Sept. 6–11.

[7] Evans, D. V., 1976, "A theory for wave-power absorption by oscillating bodies," *Journal of Fluid Mechanics*, 7 (1), 1–25.

[8] Wendt, F. et al., 2017, "International Energy Agency Ocean Energy Systems Task 10 Wave Energy Converter Modeling Verification and Validation," Proceedings of the 12th European Wave and Tidal Energy Conference, Cork, Ireland, Aug. 27–Sept. 1.

[9] WAMIT Version 7.2 User Manual, http://www.wamit.com; 2017.

[10] Newman, J. N., 1962, "The exciting forces on fixed bodies in waves," *Journal of Ship Research*, **6** (3), 10–17.

[11] Falnes, J., 2002, "Optimum control of oscillation of wave-energy converters," *International Journal of Offshore and Polar Engineering*, **12** (2), 147–154.

[12] Evans, D. V., 1981, "Maximum wave-power absorption under motion constraints," *Applied Ocean Research*, 3 (4), 200–203.

[13] Folley, M., Whittaker, T., and Henry, A., 2005, "The performance of a wave enegy converter in shallow water," Proceedings of the 6th European Wave and Tidal Energy Conference, Glasgow, United Kingdom, Aug. 28–Sept. 2.

[14] Gomes, R. P. F., Lopes, M. F. P., Henriques, J. C. C., Gato, L. M. ., and Falcão, A. F. O., 2015, "The dynamics and power extraction of bottom-hinged plate wave energy converters in regular and irregular waves," *Ocean Engineering*, **96**, pp. 86–99.

[15] Hals, J., Bjarte-Larsson, T., and Falnes, J., 2002, "Optimum reactive control and control by latching of a wave-absorbing semisubmerged heaving sphere," in *21st International Conference on Offshore Mechanics and Arctic Engineering*, Oslo, Norway, pp. 415–423.

[16] Genest, R., Félicien, B., Clément, A.H., and Babarit A., 2014, "Effect of non-ideal power take-off on the energy absorption of a reactively controlled one degree of freedom wave energy converter," *Applied Ocean Research*, **48**, pp. 236–243.

[17] A. F. O. Falcao and J. C. C. Henriques, "Effect of non-ideal power take-off efficiency on performance of single- and two-body reactively controlled wave energy converters," *Journal of Ocean Engineering and Marine Energy*, vol. 1, no. 3, 273–286, 2015.